chemosensors

MDPI

Article

Precise Integration of Polymeric Sensing Functional Materials within 3D Printed Microfluidic Devices

Jaione Etxebarria-Elezgarai [1,†], Maite Garcia-Hernando [1,2,†], Lourdes Basabe-Desmonts [1,3,*] and Fernando Benito-Lopez [2,*]

[1] Microfluidics Cluster UPV/EHU, BIOMICs Microfluidics Group, Lascaray Research Center, University of the Basque Country UPV/EHU, 01006 Vitoria-Gasteiz, Spain
[2] Microfluidics Cluster UPV/EHU, Analytical Microsystems & Materials for Lab-on-a-Chip (AMMa-LOAC) Group Analytical Chemistry Department, University of the Basque Country UPV/EHU, 48940 Leioa, Spain
[3] Basque Foundation of Science, IKERBASQUE, María Díaz Haroko Kalea, 3, 48013 Bilbao, Spain
* Correspondence: lourdes.basabe@ehu.eus (L.B.-D.); fernando.benito@ehu.eus (F.B.-L.)
† These authors contributed equally to this work.

Abstract: This work presents a new architecture concept for microfluidic devices, which combines the conventional 3D printing fabrication process with the stable and precise integration of polymeric functional materials in small footprints within the microchannels in well-defined locations. The approach solves the assembly errors that normally occur during the integration of functional and/or sensing materials in hybrid microfluidic devices. The method was demonstrated by embedding four pH-sensitive ionogel microstructures along the main microfluidic channel of a complex 3D printed microfluidic device. The results showed that this microfluidic architecture, comprising the internal integration of sensing microstructures of diverse chemical compositions, highly enhanced the adhesion force between the microstructures and the 3D printed microfluidic device that contains them. In addition, the performance of this novel 3D printed pH sensor device was investigated using image analysis of the pH colour variations obtained from photos taken with a conventional camera. The device presented accurate and repetitive pH responses in the 2 to 12 pH range without showing any type of device deterioration or lack of performance over time.

Keywords: benchtop 3D printer; colorimetric image analysis; functional materials; embedding of ionogels; miniaturised pH sensors

Citation: Etxebarria-Elezgarai, J.; Garcia-Hernando, M.; Basabe-Desmonts, L.; Benito-Lopez, F. Precise Integration of Polymeric Sensing Functional Materials within 3D Printed Microfluidic Devices. *Chemosensors* **2023**, *11*, 253. https://doi.org/10.3390/chemosensors11040253

Academic Editor: Luís Dias

Received: 6 March 2023
Revised: 5 April 2023
Accepted: 12 April 2023
Published: 19 April 2023

1. Introduction

During the last two decades, efforts have been made to reduce the size of analytical components in order to further miniaturise microfluidic devices. In this scaling down process, the size of the sensing element of an analytical device is critical. The miniaturisation of the sensing elements within microfluidic devices increases the ratio between the surface area and the volume of the sensors, resulting in improved diffusion and enhanced mass transfer through the sensing materials and accelerated response times [1]. This size reduction requires a smaller sample volume, provides accurate control of fluid flow, and ensures a homogeneous distribution of species all along the sensor [2], guaranteeing a highly controllable environment for analysis, chemically speaking, when compared to traditional sensors. The process of miniaturisation also allows for multiplexing by having a number of micro-sensors in a controlled area for the simultaneous sensing of different species, or performing the same reaction in parallel with many sensors [3,4]. Multiplexing can also lead to barcode sensing, in which the final result of the analysis comes from the combination of all the sensing outputs [5,6]. Therefore, recent developments in portable and disposable analytical instrumentation reveal an increasing interest in the integration of sensing materials [7–9] and functional materials to act as pumps and valves in microfluidic systems [10–12]. However, there is still a high demand for truly integrative strategies that

are simple to implement and enable functional materials to be adequately coupled within LOC devices [9,13].

Recently, 3D printing technology is gaining more attention than similar techniques used for the integration of materials or reagents within microfluidic devices, such as inkjet printing [14] or non-contact microarrayers [15]. 3D printing technology enables rapid design iterations and fast optimisation during the development of the technology, offering great advantages over traditional microfabrication techniques such as photolithography, soft lithography, xurography, hot embossing, etc. [16–18]. 3D printing has been used for the integration of materials or reagents within microfluidic devices through microfabrication, such as microfabricated valves and pumps [19] or 3D cell culture with customised cell distribution, heterogeneity, or tissue-specific functions [20]. Such approaches are successful for the printing of multiple materials, but they require modifications to the printers or the chemical composition of the material to be printed in order to adapt them to the specific fabrication needs, both of which complicate and increase fabrication costs.

Recent developments in assembly-free fluidic valves and pumps have been demonstrated within 3D printed microfluidic devices [21], as well as 3D printed smart sensing materials [22,23] and functional materials [24–26] in microfluidic systems. These types of materials provide new functionalities for in situ operations, fulfilling the needs of more autonomous and easy-to-use devices, which may lower energy consumption and, thus, improve operability compared to traditional benchtop and microfluidics systems [9]. In particular, ionogels are polymeric hybrid materials that have generated interest for their potential in sensing applications [27]. They incorporate an ionic liquid (IL) within the polymer matrix, resulting in a polymeric network that combines the properties of both the three-dimensional solid structure of the polymer and the negligible vapour pressure and thermal stability of the immobilised IL. ILs also present high solvation power as they are able to dissolve substances that are difficult to dissolve in conventional solvents (monomers, cross-linkers, etc.) [28]. There is an endless number of ILs with different natures, so the chemical and physical properties of the ionogel can be adjusted by simply changing the IL [29]. In addition, ionogels can be tailored to be photopatternable for in situ polymerisation and tuned to integrate other molecules within their matrix to acquire new functionalities [9,30]. Among others, colorimetric sensors are a great example of the integration of functional materials in microfluidic analytical devices for sensing applications [23].

Colorimetric sensors allow us to translate the output either by the naked eye or by using optical instruments, so their simplicity and versatility facilitate their implementation in microfluidic and portable devices. Colorimetry offers a more affordable and user-friendly sensing approach with adequate data collection and imaging [31]. In particular, the HSV colorimetry system has been used to quantify colour events in microfluidic devices [32,33]. HSV is a transformation of the traditional RGB, where the hue component (H) defines the colour represented by a number from 0 to 360 that corresponds to a position on a colour space coordinate diagram, defining a unique and precise colour. The other two coordinates of the system correspond to intensity (S) and darkness (V). Hue is stable and easy to calculate, making it a useful tool for colorimetric sensing applications in microfluidic analytical devices [23,34].

Considering the technological limitations during the integration of functional materials within 3D printed microfluidic devices, we present a specially designed microfluidic architecture that allows for the easy integration of multiple materials within 3D printed microfluidic devices in the form of discrete sensing zones with controlled dimensions, which avoids assembly errors. The fabrication uses 3D printed T-shaped cavities in the channel for the easy, in situ, and precise integration of polymerisable materials, with no need of surface functionalisation. The technique simplifies the manufacturability of hybrid 3D printed microfluidic devices. Moreover, our approach combines the use of conventional 3D printing equipment with a smart design strategy, which plays an essential role in the integration of hydrophilic functional materials on hydrophobic or organophilic materials, without any prior surface treatment. As a proof of principle, the proposed strategy was

used to embed four pH-sensing ionogels, all of different chemical compositions, in order to provide pH measurements over a wide range of pH values and within the microchannels of hybrid microfluidic devices.

2. Experimental Section

2.1. Fabrication of the Chip by 3D Printing

The design and a real picture of the microfluidic device is depicted in Figure 1a. The device featured internal microfluidic channels directly connected to external connectors. The three female-luer connectors, two at the inlet and one at the outlet, allowed for the connection of the main microfluidic channel with external fluidic sources due to it being compatible with P-675 male luer to 1/4-28 female connector and with Barb to Slip-Type male luer adapters (Fisher Scientific, Waltham, MA, USA). The main channel featured an open channel section that was 32 mm long, 700 μm wide, and 700 μm high, located on the top side of the device, which was closed with a pressure-sensitive adhesive layer (PSA) (Adhesive Research, Limerick, Ireland) when in operation. The other four small connectors, with internal cone shapes of D_1 = 1.3 mm, D_2 = 1 mm, and H = 3 mm, were specially designed to allow for the precise coupling of pipette tips for the leak-free pipetting of viscous materials. These connectors, together with the adjacent internal channels, were arranged perpendicularly to the main channel, and aimed to facilitate the integration of the material of interest. The adjacent integration channels and the main microfluidic channel were connected using three-dimensional T-shaped cavities that allowed the pipetted material to be embedded and anchored on the walls of the reservoirs fabricated on the bottom side of the main microchannel (Figure 1b). This structure consisted of an internal channel that was 11.2 mm long and 1 mm in diameter, and a T-shaped cavity of 2.2 μL. The total volume that was to be integrated in to this structure was 12.4 μL. Therefore, the four pH-sensing ionogels were integrated within the T-shaped anchorage structure, leading to strategically positioned sensing zones, of 0.5 mm^2 surface area, at the bottom of the main channel (Figure 1c). A Y-shaped channel and a serpentine were included at the inlet to enable simultaneous injection and the mixing of two reagents so that chemical reactions could be performed inside the meandering channel section located before the sensing zones of the device. The Y-shaped channels were 15.8 mm long, 500 μm wide, and 600 μm high, and the meandering channel was 44 mm long, 700 μm wide, and 700 μm high.

3D printing technology was used to manufacture the microfluidic device. It consists of a light-based stereolithography (SLA) 3D printer (Formlab 1+, Formlabs, U.S.) process that builds individual layers of a model with a liquid polymer by hardening it with a laser beam. Creo Parametrics 2.0 CAD software was used to design 3D models of the microfluidic device (Figure 1a), and PreForm software was used to build the supporting structures that allow for satisfactory printing of the devices (see Figure S1). The device was 3D printed as a single piece, in acrylic material (Clear resin FLGP CL02, Formlabs, Somerville, MA, USA), using a 50 μm printing resolution. After printing, the obtained structure was rinsed in isopropyl alcohol (Scharlabs, Barcelona, Spain) for 4 min in order to eliminate the uncured resin from the cavities and was subsequently post-cured under 365 nm UV light using an EF-180C handheld UV lamp (Spectroline™, Hampshire, UK), for 15 min. Then, the holders were removed from the microfluidic devices with a snip and the final devices were wet-sandpolished to enhance transparency. Once the sensors were integrated within the channel, the devices were sealed with a PSA layer (Adhesive Research, Limerick, Ireland). Luers (Microfluidics ChipShop, Jena, Germany) and tubing (Altmann Analytik GmbH & Co., München, Germany) were used to make a functional microfluidic device and introduce the liquid samples.

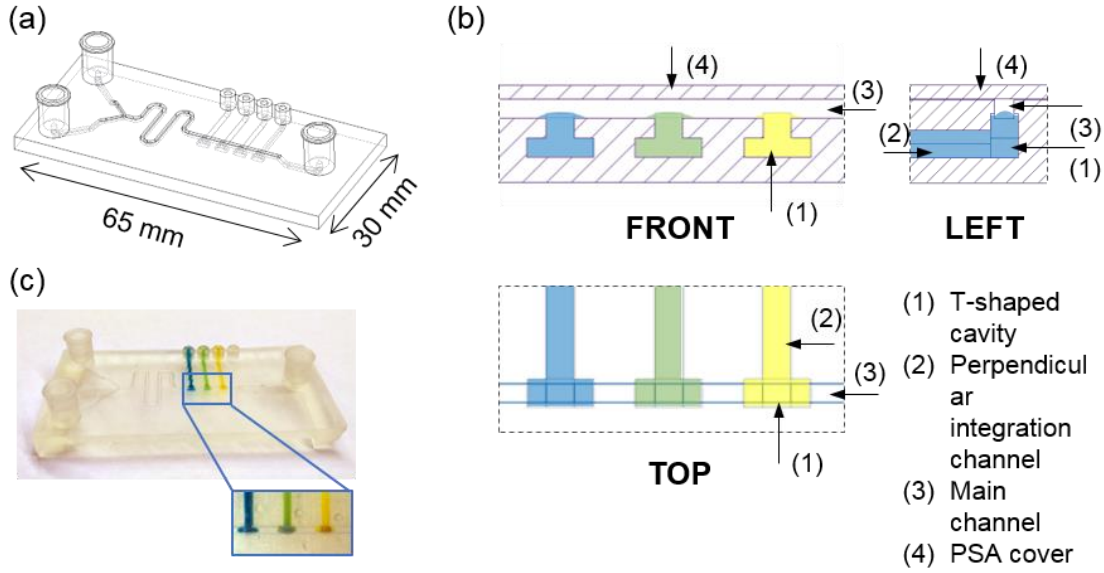

Figure 1. (**a**) 3D model representation of the microfluidic device. Internal channels and cavities are shown as hidden lines, drawn with a lighter greyish black, while external channels are represented with a darker black. (**b**) Representation of the T-shaped sensing zones (front, left and top views). (**c**) Picture of the 3D printed device with integrated pH-sensing ionogels (from left to right, bromocresol green (BG), bromocresol purple (BP), phenol red (PR), and phenolphtalein (Ph)).

2.2. Ionogels Synthesis and Integration

For the synthesis of the prepolymer solution, the four basic components and the two ILs were purchased from Sigma Aldrich (Madrid, Spain). As the monomer, poly(*N*-isopropylacrylamide) (pNIPAAm) was used, dimethoxy-2-phenylacetophenone (DMPA) as the photoinitiator and *N*,*N*′-methylenebisacrylamide (mBAA) as the crosslinker. The three components were solubilised in two ionic liquids. 1-ethyl-3-methylimidazolium ethyl sulphate (EMIES) was used for bromocresol green (Scharlab, Barcelona, Spain), phenol red and phenolphthalein (Sigma Aldrich, Madrid, Spain) sensors, and trihexyltetradecylphosphonium dicyanamide (DCA) for bromocresol purple (Acros Organics, Madrid, Spain) sensor. The prepolymer solution of each pH sensor was comprised of NIPAAm monomer, DMPA, mBAAm crosslinker, IL and a pH indicator (BG, BP, PR or Ph). The molar relation was the same in all the sensors: 40:2:1 (NIPAAm:DMPA:mBAAm), but different for the pH indicators and the ILs, as indicated in Table 1. The crosslinker, IL, and pH indicators were mixed at 80 °C under stirring conditions until fully dissolved. For the PR sensor, 60.0 µL of NaOH, 0.01 M, and 20.0 µL NaOH, 1M, were added to the mixture at continuous stirring.

Table 1. Chemical composition of the different ionogel materials used for the fabrication of the pH sensors.

pH Indicator / Ionic Liquid	NIPAAm (mg)	mBAAm (mg)	DMPA (mg)	pH Indicator (mg)	Ionic Liquid (mL)
BG/EMIES	452.0	30.9	30.0	5.0	2.0
BP/DCA	452.0	30.9	30.0	5.0	1.5
PR/EMIES	452.0	30.9	30.0	5.0	1.0
Ph/EMIES	452.0	30.9	30.0	7.0	2.0

The integration of the sensing materials was carried out by loading 13.0 µL of the different ionogel precursor cocktails from the four pipette-tip connectors to the T-shaped structures, and the cocktails were subsequently photopolymerised under UV light at

365 nm (EF-180C hand-held UV lamp, Spectoline, Hong Kong, China) for 45 min. Once polymerised, the ionogels were rinsed with isopropanol and distilled water in order to eliminate any non-polymerised material. After polymerising, the ionogel containing BP was soaked in a concentrated solution of BP in ethanol, 1.0 µL of the solution, for 15 min in order to improve its colour response. To prepare the BP concentrated solution, 10.0 mg of BP powder were dissolved in 10.0 mL of ethanol. Finally, the device was sealed with a PSA layer to generate a fully functional microfluidic device for pH sensing.

2.3. Set-Up and Imaging

The device was characterised using the set-up shown in Figure 2**.** It consisted of a syringe pump, Standard Infuse/Withdraw Pump 11 Elite Programmable Syringe Pump (Harvard apparatus, Cambridge, MA, USA), to drive the liquid through the device, a microscope with an integrated camera (ISH500 Tucsen Photonics, Fujian, China), and a software application (TCapture, Tucsen Photonics, Fujian, China) for image acquisition. The samples were reproducibly illuminated using a light source composed of a LED lamp (MKM012405WH1, 25W, ADEO, Ronchin, France) and a LED ring-light in a homemade white chamber, which ensured the same light conditions during the picture/video acquisition process. The captured images were saved in a TIF format with a resolution of 2584 × 1936 pixels. Then, a region of interest (ROI) of 120 by 120 pixels (0.5 mm^2) was chosen from each of the sensor surfaces for analysis. The white balance settings of the microscope camera were kept constant during the experiments. ImageJ (1.53 t 24 August 2022, NIH), software was used to determine the RGB colorimetric parameters of each pH sensor ionogel, and from those, Hue (from HSV system) was then calculated using Wolfram Alpha (https://www.wolframalpha.com/ (accessed on 1 April 2019)), in order to obtain the colour of the ionogel.

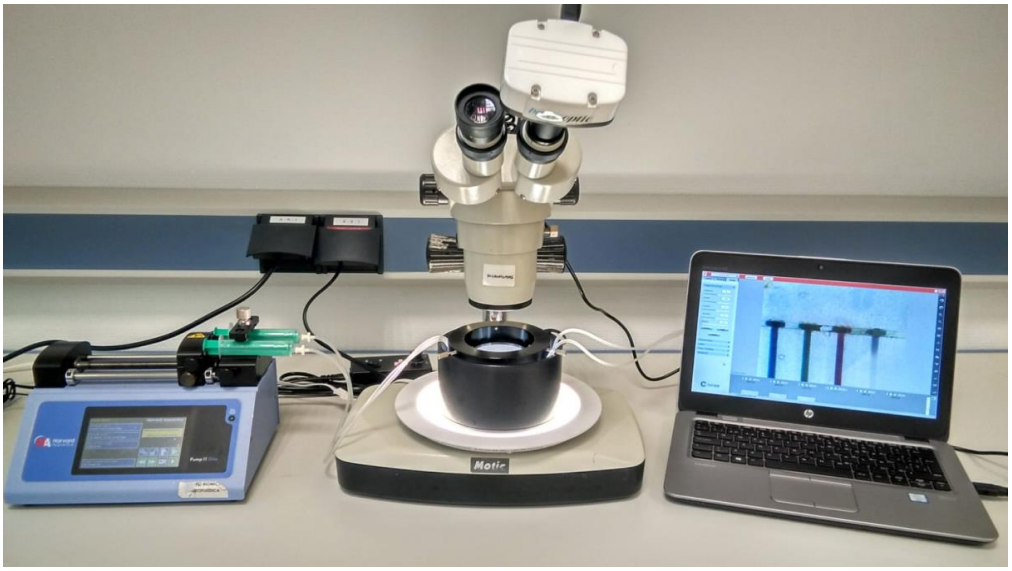

Figure 2. Set-up used for the characterisation of the sensor.

2.4. pH Sensor Colorimetric Characterisation

The pH-sensing performance of the ionogels was characterised by flowing solutions at different pHs and flow rates (2–600 µL min^{-1}) through the 3D printed microfluidic device using the pump. The pH solutions were prepared using HCl for the acidic ones (from 1 to 7) and NaOH for the alkaline ones (from 8 to 14) (Sigma Aldrich, Madrid, Spain). For the acidic series, pH 1 solution was first prepared making an HCl 0.1 M solution in distilled water, and subsequent pH solutions were made with a 1:10 dilution of the previous pH solution. To prepare the pH solutions of the basic series, the same procedure was followed. First, NaOH 1 M (pH 14) was prepared, and sequential 1:10 dilutions were made until

pH 8 solution was reached. Then, the acquired images for each pH value and sensing zone were analysed, as previously explained. Finally, the operation ranges were defined for the four pH sensor ionogels. A Milwaukee pH-51 (Barcelona, Spain) pH-meter was used to measure the pH of each solution.

3. Results and Discussion

3.1. Microfluidic Device Fabrication

The printing process was optimised to enable internal and superficial channels and internal T-shaped features by means of a conventional stereolithography 3D printing method (see Figure S1). Model orientation and supporting structures are of utmost importance to generating successful printings of complex features containing internal cavities [35]. Supporting structures were found to be important to give physical support to the 3D printed features and to avoid the non-homogeneous shrinkage and compression of bottom layers in the case of models that contain a flat surface. Therefore, an incorrect orientation of any of the parts led to internal microchannel clogging; thus, a proper orientation was necessary to enable the draining of the uncured resin trapped inside the microstructures. Figure S1 shows adequate orientation and supporting structures for a satisfactory 3D printed device, with the most critical features, with the deepest cavities, and at the uppermost plane. They were printed at the last moment to avoid the clogging of the cavities. We also considered the printing time and removal of the uncured resin before bringing the printed part to ambient light to avoid clogging the internal structures. To solve all the problems stated above, the printing conditions were optimized so that the supports were distributed periodically with a high occupancy density over the entire bottom side of the part, which was oriented with an angle of 30° to the horizontal axis and 20° to the vertical axis. This way, the resulting contraction for the printed part, after UV polymerization, was seen to be homogeneous and negligible for the proposed application.

The microfluidic structures could also be fabricated by microfabrication techniques such as lamination or the popular method of soft lithography, but these are more laborious techniques. They require precise alignment and bonding of more than one part to generate the final device, as in this case, which demanded internal structures. Moreover, due to the high hydrophobicity of PDMS devices, ionogels did not deposit well in channels. 3D printing is based on loading the design and waiting for the result, which facilitates any possible change needed in the design, while for techniques such as soft lithography, a design change begets longer fabrication steps after the modification of the design. The lack of alignment steps is also a major advantage of 3D printing, which, in our case, just required a polishing step to smoothen the surface of the device and the adhesion of a PSA layer to close the channel.

The use of an open channel aimed to increase the transparency of the device in the positions where colorimetric measurements were needed. This type of resin is highly transparent after fabrication, but it suffers from aging over time, developing a yellowish colour [33]. This considerably reduced the transparency of the material, so the colour would not be accurately measured over time. Although several 3D printable resins are catalogued as optically clear, such as the FLGP CL02 resist used in this work, their transparency depends on the roughness of the surface, making these materials translucent at best but not fully transparent [18]. Therefore, in order to avoid the aforementioned transparency issues, the open microfluidic channel was fabricated and subsequently sealed using PSA to enhance optical transparency. PSA is a transparent film that does not lose its transparency, and if it becomes damaged, it can be easily replaced by another PSA layer.

3.2. Integration of pH-Sensitive Ionogels in the 3D Printed Microfluidic Device

Our strategy to integrate functional materials in 3D printed microfluidics devices involved the combination of T-shape cavities with UV-photopolymerisable sensors. This method facilitated the precise positioning of the sensing materials inside the microfluidic

channel without the need to use the complex 3D printing of multiple materials processes or spotters [36].

To evaluate the efficacy of the proposed strategy, we compared the shape and adhesion strength of ionogels loaded and polymerised either within T-shaped anchoring structures or directly on the surface of microfluidic channels (Figure 3a). We added 2.2 µL of the four pH-sensitive ionogels in both the conventional rectangular channel and by using the T-shape cavities. After UV-polymerisation of the ionogels, the microfluidic channels were closed with the PSA layer and the device was connected to the pump. Well-defined and regular ionogel shapes with the T-shape cavities were obtained. However, we observed inhomogeneous sensing sections with different shapes, areas, and heights in the microchannel (without the T-shape cavities) after ionogel polymerisation.

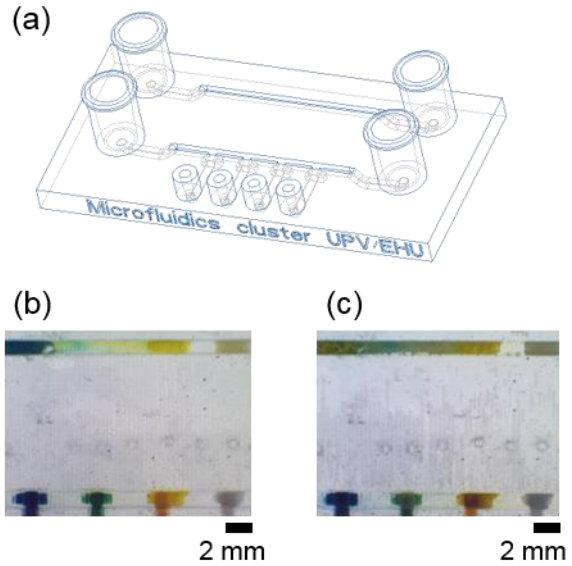

Figure 3. Adhesion tests performed to analyse the importance of the proposed architecture on the robustness of the integrated pH sensors. (**a**) 3D model representation of the microfluidic device, in which two different 3D printed structures were compared: a simple channel (top channel) and the proposed T-shaped well architecture (bottom channel). Images show the integration of the materials (**b**) right after polymerisation and rinsing with distilled water and (**c**) after 2 min flow at 600 µL min^{-1}, pH = 6.

To test the adhesion of the gels within the channel, flow was increased from 100 to 600 µL·min^{-1}. All the ionogels immobilised within the T-shape structures remained attached and stable. In the channels, on the other hand, the pH sensor with BP, which contains a hydrophobic ionic liquid (DCA), easily detached from the microchannel during the rinsing step with distilled water (Figure 3b,c). The other three pH sensors, with the hydrophilic ionic liquid (EMIES), remained attached to the channel surface. The results demonstrated that the integrated T-shape cavities increased the anchoring capacity of the materials, avoiding surface functionalisation and enabling the integration of sensing zones with a well-defined shape, regardless of their chemical composition. The T-shaped configuration provided a precise positioning of all the pH sensors, with reproducible sensing areas previously defined during the microfluidic designing step.

This strategy had important implications as the inhomogeneity of the sensing area impacted on the sensor performance and on the obtained results. This is even more important for colorimetric sensors where the colour distribution on the sensing surface should be homogeneous. Obviously, the sensors generated on the conventional channels were not able to provide good responses over time, and results were not reproducible from device to device, leading to high pH value deviations over equal sensors.

In the case of the pH sensors, the diffusion of protons through the sensing matrix is important to control their response time. Therefore, in the sensors fabricated in the channel, their response to pH variations was random. On the other hand, in the T-shape sensors their response was homogeneous and repetitive in all of the sensing areas, regardless of their chemical composition and device. Therefore, the results evidenced that this fabrication protocol ensured reproducibility in size and shape during the manufacture of the polymer sensing areas within 3D printed microfluidic networks, and thus, a homogeneous and repetitive sensor response.

It is important to note that the chemistry of the ionogel influenced the integration process, e.g., DCA versus EMIES IL, evidenced the need of functionalisation steps when using ionogels in conventional microfluidic channels. The adhesion results presented in Figure 3 demonstrate that a surface functionalisation treatment was necessary to create stable ionogel microstructures with defined dimensions and shapes, as previously reported in the section discussing conventional channels [34]. The functionalisation of the surface of a microfluidic device in a specific location of the channel is a complicated task, and it becomes more complicated for microfluidic devices fabricated by 3D printing due to the nature (chemistry) of the printing materials, resins, and the device fabrication protocols, making these types of sensing capabilities impractical. However, when the T-shape architecture was combined with photopolymerisable materials, these limitations were overtaken. In addition, in precise locations, T-shape cavities were suitable for loading viscous ionogel solutions and generating sensors after in situ polymerisation.

3.3. pH Sensing with the 3D Printed Microfluidic Device

The performance of the device (four sensing areas) at different pHs is presented in Figure 4a and Table S1. We observed an immediate colour change in the middle of the sensor (<1 s) that spread over the whole sensor in 2 min. The Hue value of 0.5 mm^2 ROI slightly varied during this time period. Therefore, a measurement was taken after 2 min to ensure we had a homogeneous colour distribution in the whole sensor surface and a repetitive Hue value from device to device. It needs to be highlighted that a 2 min detection time is not a limiting factor, as smaller ROIs can be selected in the middle of the sensor surface, enabling faster analysis times.

According to the results presented in Figure 4b, each sensing area had a characteristic sensing performance, showing a colour change at a specific pH value. The BG sensor showed an evident colour switch from pH 2 to 4 (pK_a of 2.0, see SI Section "ionogel pH sensor performance" and Table S1, for further explanation) [5,37–39], with a less pronounced variation of the Hue value, 200 $\pm$ 25, from pH 6, which was considered as the plateau value for this particular sensing area. The BP sensor displayed a colour switch from pH 4 to 9 (pK_a of 5.9) with pseudo plateau values of 75 $\pm$ 25 and 225 $\pm$ 25, before and after switching. On the other hand, the colour switch of PR and Ph sensors underwent drastic changes to purple at pH 9–10 (pK_a of 9.5) and at pH 10–11 (pK_a of 10.4), respectively. We observed that, for acidic pH values, the colour did not change for both sensors, which corresponded to the behaviour of these types of indicators in solution. For instance, the PR has low solubility in acidic and neutral media but is soluble in alkaline solutions, showing a 6.8–8.2 gradual pH transition from yellow to purple. Therefore, the prepolymer solution containing PR was slightly alkalinised before polymerisation in order to improve the solubility of PR (experimental Section 2.2). The four sensing areas, when used as a barcode sensor, enabled the measurement of the whole pH range of the solution passing through the microchannel, from pH 2 to 12.

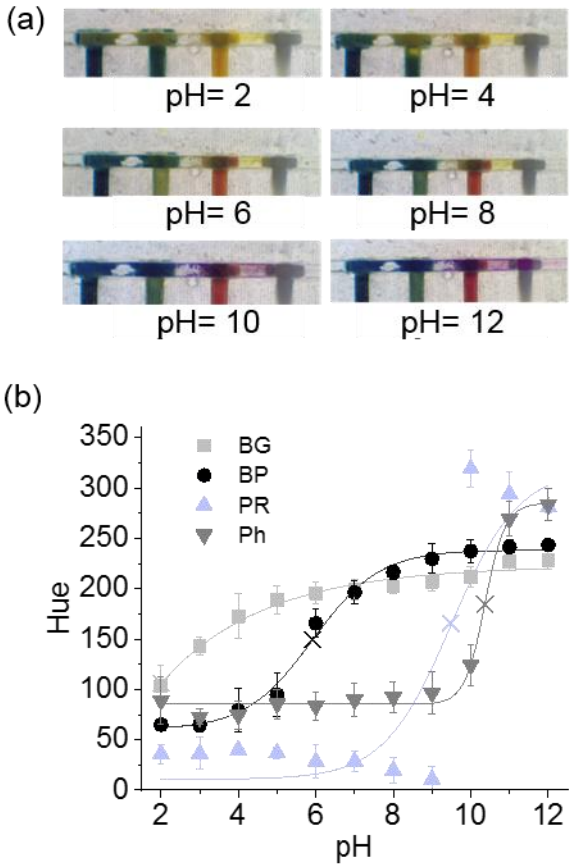

Figure 4. (**a**) Images of the barcode pH sensor are of the microfluidic device for six pH conditions, ranging from 2 to 12. (**b**) Hue (*H*) values for each ionogel pH sensor, when varying the pH from 2 to 12, and the pK_a values for each sensor (x). Error bars correspond to the mean values ± SD (n = 3) for three different devices, which were fabricated at different times, using fresh ionogel solutions each time.

The transition ranges reported in the literature for the pH indicators in solution used in this work are 3.8–5.4 for BG, 5.2–6.8 for BP, 6.8–8.2 for PR, and 8.2–10 for Ph [40]. These values are slightly different from the ones found by us. We previously reported the deviation in the response range of the pH indicators in the ionogel from their expected values in solution, and this deviation was attributed to the immobilisation of the indicators in the gel-like structure [5].

It is worth mentioning that, for the four sensing areas, the biggest deviations in Hue values occurred at pH values that were close to the switching point of each indicator. At those points, local variations on the colour, brightness, and shadowing at different locations of the sensor surface were observed due to the inhomogeneity of the ionogel surface. This led to a less homogeneous colour and a higher Hue value error. Other types of image analysis techniques could be used in order to reduce this systematic error.

3.4. pH Sensing Performance

In order to validate the barcode sensor performance in the 3D printed microfluidic device, a simple acid–base reaction was performed. An acidic solution, 0.1 M HCl, was introduced in one of the inlets and a basic solution, 0.1 M NaOH, was passed through the other inlet at a flow rate of 150 $\mu L \cdot min^{-1}$. These two solutions were mixed in the serpentine where the acid–base reaction took place, as seen in Figure 5. Then, the pH value of the solution was estimated from the calibrated Hue values of each sensor. This was done by fitting the calibration curves to sigmoidal equations to meet the solutions given by the Henderson–Haseelbach Equation [5]. The equations were resolved using Solver, a program

that uses an iterative method to perform calculations for finding a solution that satisfies all the constraints defined, thus obtaining the pH values for each Hue value read from the ionogel sensing areas, see SI Section "ionogel pH sensor performance" and results from Table S2, for further explanation. Finally, after the reaction occurred, the value was compared to the pH value of the solution obtained with a commercial pH-meter (7.0).

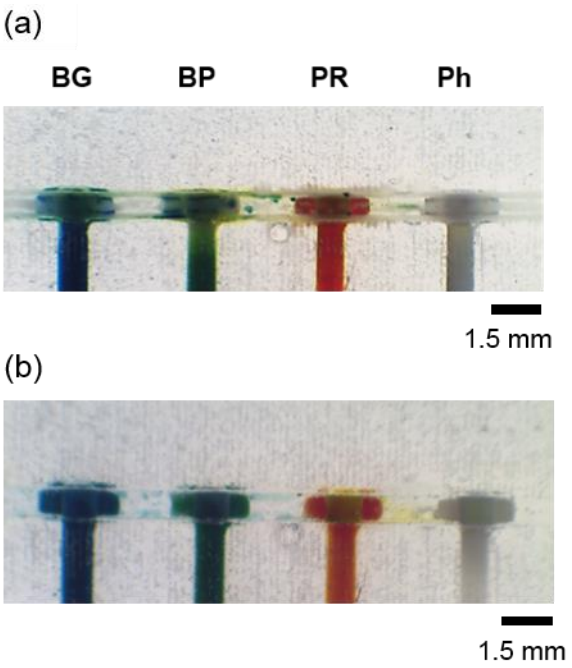

Figure 5. Picture of the section of the pH sensor device (**a**) after washing it with DI water and (**b**) after the reaction of an equimolar mixture of HCl and NaOH was performed inside the meandering channel and passed through the sensing areas.

Hue values of the sensing areas were calculated to be 211 for BG, 206 for BP, 25 for PR, and 87 for Ph, and were compared with the Hue values given by those sensing areas during the characterisation process (Figure 5b and Table S2). According to the results obtained from the fitted equations, the Hue values obtained from the sensing areas were 7.5 for BG, 7.2 for BP, 6.9 for PR, and 6.8 for Ph. The average pH value for the acid/base reaction performed in the microfluidic device for the four sensing areas was 7.1 $\pm$ 0.3, according to the MATLAB fittings (see Table S2). An accuracy of 0.1, RE (%) = 1.4%, was obtained when comparing this result with the one obtained using the benchtop pH-meter.

Several studies reported the development of microsystems for pH sensing with the sensors in suspension [41,42] or with surface sensors [43]. They showed short response times and good sensitivity, but they required expensive and specialised equipment such as fluorescence or an optical spectrometer, photodiodes, and a laser. SERS measurements of smart-nano-in-micro particles showed a sensitivity of 0.2 in pH variation but required sample handling to collect the particles and measure their response under specialised equipment. Moreover, there was a lack of real-time measurement because of the time gap due to handling [41]. Moradi et al. reported a fluorescence-based microfluidic pH sensor which was sensitive and performed real-time measurements, but it required specialised equipment to induce and measure fluorescence [43]. Lu et al. suggested a colorimetric surface-sensing approach for pH monitoring for pH < 3 and pH > 6 [41]. Similar to our work, they combined a colorimetric pH indicator with a polymeric membrane, but they collected the data and transformed it into voltage by following a complex process. The surface sensor relied on trapping the membrane between the bottom and the upper part of the device, which complicated the device fabrication. Therefore, our work offers a colorimetric pH measurement tool with dynamic fabrication features that does not require

expensive or specialised equipment for the data analysis, demonstrating its unique place within pre-existing technology.

These things considered, the barcode ensures four simultaneous measurements in a simple way. Their combination should match with one of the combinations obtained in the calibration. Therefore, if one of the sensors does not work properly, it could be easily detected due to a mismatch with the other three measurements.

3.5. 3D Printed Microfluidic Device Reusability

The performance of the device was investigated over time by measuring the Hue of the four sensing areas at two different pH values for fourteen times using a strong acid solution (pH 2) followed by a strong basic solution (pH 12). A pH 2 solution was introduced through the inlet and, after 2 min, the Hue values were measured. Then, the basic solution was introduced, also measuring the colorimetric response after 2 min (Figure 6).

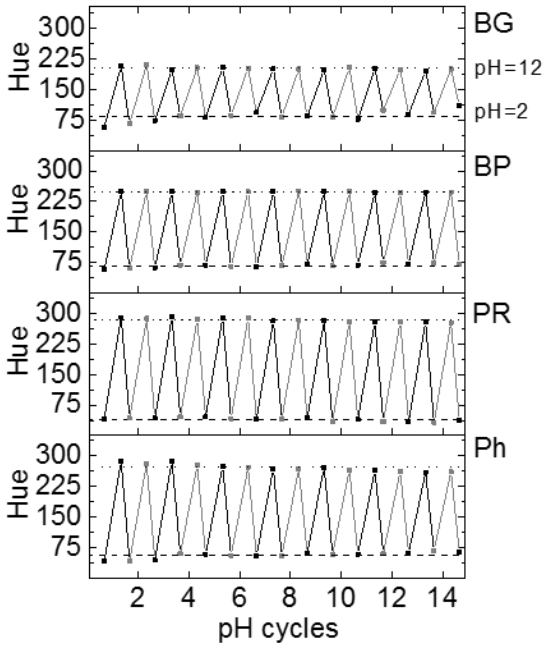

Figure 6. Hue values at pH 2 and pH 12 for 14 cycles of passing through the sensing areas using an acidic solution followed by a basic solution. The Hue values were obtained after 2 min stabilisation time. The dashed and dotted lines indicate the average of the Hue values from all of the cycles for each sensor at pH 2 and 12, respectively.

BP and PR presented the best repetitiveness, showing little deviation from the average value for all of the cycles. BP displayed really good repetitiveness values during the 14 cycles, showing Hue values of 68 ± 5 for pH 2 and 249 ± 1 for pH 12. Regarding PR, Hue values were also stable, 40 ± 5 for pH 2 and 284 ± 5 for pH 12, see Figure S2.

When it comes to BG and Ph, both sensors displayed lower stability after the 14 cycles. BG gave a stable signal for pH 12 during all the cycles, showing a Hue signal of 201 ± 4, while at pH 2, the signal started to decrease from cycle 12 on, showing a Hue of 85 ± 16. On the other hand, Ph ionogel presented a less repetitive performance. Indeed, the Hue value at both pH's did not recover the original values after the third cycle. This tendency can be observed in Figure 6. The Hue values were 57 ± 8 for pH 2 and 271 ± 9 for pH 12 (see Figure S2).

It must be highlighted that the pH indicators that do not fully recover the initial Hue values were the BG, responding in a pH range of 1–3, and the Ph, responding in a pH range of 10–12. In contrast, BP (responding to pH 5–9) and PR (responding to pH 9–11) recovered the colours well during the 14 cycles (pH 2 to 12). In an attempt to explain this, we speculate that the accumulative effect of protons from the pH 2 solution was not fully

neutralised with the base of the pH 12 solution, varying the BG and the Ph colours at those extreme pHs. On the other hand, BP and PR responded well to those two pH value changes during the 14 cycles in a reversible way, with Hue values of low deviation, showing great recovery and performance since the colour change was far from the two extreme pH values investigated. Additionally, the fast and homogenous colorimetric response from the indicators demonstrated an adequate diffusion of protons through the ionogel polymeric matrix (~0.01 cm^2 s^{-1}).

4. Conclusions

The proposed strategy aims to simplify the task of integrating functional materials within 3D printed microfluidic devices. It combined a 3D printed smart architecture and the in situ integration of photopolymerisable functional materials with integrated sensing moieties within their polymeric matrixes. The main advantage of this was the simplicity of the integration procedure, making the process user-friendly and accessible to many end users from different scientific fields.

The enhanced adhesion obtained due to the anchoring characteristics of the architecture avoided the need for any chemical functionalisation on the surface for the generation of precise and stable sensing zones. The reproducible dimensions of the sensing zone minimised assembly errors and enhanced sensing performance. Moreover, this strategy combined two stand-alone techniques, in situ photopolymerisation of functional materials and 3D printing, so it did not require any modification of conventional printers, printing resins, or the integrated functional materials.

This integration protocol was demonstrated for a miniaturised pH sensor barcode composed of four pH sensing areas, all of different chemical compositions, where each sensing area aimed to provide a high-performance resolution in a specific pH range, while all sensing areas together covered the whole pH range. The possibility of producing multiple sensing areas along the main channel opens multiplexing capabilities. Moreover, other biorecognition elements (enzymatic assays, antibodies, biomolecules, etc.), could be incorporated within the polymer matrix, covalently or by ionic interactions, in order to extend the toolbox of materials and biosensors, and thus, the sensing capabilities of the device [23,44–46].

The dimensions and design used in this work enabled easy data collection and colorimetric analysis with no specialised equipment, but we would like to highlight the versatility of the technique. The system could be used with different design configurations for many applications. For instance, by integrating other types of functional materials, the fabricated areas could be used as actuators [47]. Moreover, the dimension of the areas is just limited by the printer parameters and the chemistry of the sensor.

Furthermore, this fabrication method used conventional bench-top 3D printing, offering the advantage of rapid fabrication cycles, which led to reduced costs and enhanced efficiency, allowing for the agile production of complex geometries to bridge the gap between new ideas and the generation of prototypes for design optimisation. This enabled us to achieve optimised and accelerated transitions from prototype to product, in a cost-effective way, reducing the risks associated with manufacturing.

Supplementary Materials: The following are available online at https://www.mdpi.com/article/10.3390/chemosensors11040253/s1, Figure S1: Image of a printing model that includes a supporting structure and proper model orientation; Table S1: Hue values given by BG, BP, PR, and Ph sensors for pH values from 2 to 12. Error bars correspond to mean values ± SD (n = 3); Ionogel pH sensor performance including Table S2: Fitting data for the calibration curves of BG, BP, and PR; Matlab code [5,37–39].

Author Contributions: Conceptualization, J.E.-E., M.G.-H., L.B.-D. and F.B.-L.; methodology, J.E.-E., M.G.-H., L.B.-D. and F.B.-L.; software, J.E.-E.; validation, J.E.-E. and M.G.-H.; formal analysis, J.E.-E. and M.G.-H.; investigation, J.E.-E., M.G.-H., L.B.-D. and F.B.-L.; resources, L.B.-D. and F.B.-L.; data curation, J.E.-E. and M.G.-H.; writing—original draft preparation, J.E.-E. and M.G.-H.; writing—

review and editing, J.E.-E., M.G.-H., L.B.-D. and F.B.-L.; visualization, L.B.-D. and F.B.-L.; supervision, L.B.-D. and F.B.-L.; project administration, L.B.-D. and F.B.-L.; funding acquisition, L.B.-D. and F.B.-L. All authors have read and agreed to the published version of the manuscript.

Funding: This research was founded by the University of the Basque Country (ESPPOC 16/65 and PIF16/204), "Ministerio de Ciencia y Educación de España" grant PID2020-120313GB-I00/AIE/10.13039/501100011033, and "Gobierno Vasco" grant IT1633-22.

Institutional Review Board Statement: Not applicable.

Informed Consent Statement: Not applicable.

Data Availability Statement: Not applicable.

Acknowledgments: The authors would like to acknowledge Adhesive Research for providing PSA sheets. F.B.L. and L.B.-D. acknowledge the "Red de Microfluídica Española" RED2018-102829-T.

Conflicts of Interest: The authors declare no conflict of interest.

References

1. Ali, M.A.; Hu, C.; Yttri, E.A.; Panat, R. Recent Advances in 3D Printing of Biomedical Sensing Devices. *Adv. Funct. Mater.* **2023**, *32*, 2107671.
2. Derkus, B. Applying the miniaturization technologies for biosensor design. *Biosens. Bioelectron.* **2016**, *79*, 901–913. [CrossRef] [PubMed]
3. Herranz, S.; Marciello, M.; Marco, M.-P.; Garcia-Fierro, J.L.; Guisan, J.M.; Moreno-Bondi, M.C. Multiplex environmental pollutant analysis using an array biosensor coated with chimeric hapten-dextran-lipase constructs. *Sens. Actuators B Chem.* **2018**, *257*, 256–262. [CrossRef]
4. Lee, J.; Haddon, D.J.; Wand, H.E.; Price, J.V.; Diep, V.K.; Hall, D.A.; Petri, M.; Baechler, E.C.; Balboni, I.M.; Utz, P.J. Multiplex giant magnetoresistive biosensor microarrays identify interferon-associated autoantibodies in systemic lupus erythematosus. *Sci. Rep.* **2016**, *6*, 27623. [CrossRef]
5. Curto, V.F.; Fay, C.; Coyle, S.; Byrne, R.; O'Toole, C.; Barry, C.; Hughes, S.; Moyna, N.; Diamond, D.; Benito-Lopez, F. Real-time sweat pH monitoring based on a wearable chemical barcode micro-fluidic platform incorporating ionic liquids. *Sens. Actuators B Chem.* **2012**, *171–172*, 1327–1334. [CrossRef]
6. Cardozo, N.; Zhang, K.; Doroschak, K.; Nguyen, A.; Siddiqui, Z.; Bogard, N.; Strauss, K.; Ceze, L.; Nivala, J. Multiplexed direct detection of barcoded protein reporters on a nanopore array. *Nat. Biotechnol.* **2022**, *40*, 42–46. [CrossRef]
7. Mugherli, L.; Lety-Stefanska, A.; Landreau, N.; Tomasi, R.F.-X.; Baroud, C.N. Quantifying the sol–gel process and detecting toxic gas in an array of anchored microfluidic droplets. *Lab Chip* **2020**, *20*, 236–243. [CrossRef]
8. Czugala, M.; Gorkin, R., III; Phelan, T.; Gaughran, J.; Curto, V.F.; Ducrée, J.; Diamond, D.; Benito-Lopez, F. Optical sensing system based on wireless paired emitter detector diode device and ionogels for lab-on-a-disc water quality analysis. *Lab Chip* **2012**, *12*, 5069–5078. [CrossRef]
9. Catalan-Carrio, R.; Saez, J.; Fernández Cuadrado, L.A.; Arana, G.; Basabe-Desmonts, L.; Benito-Lopez, F. Ionogel-based hybrid polymer-paper handheld platform for nitrite and nitrate determination in water samples. *Anal. Chim. Acta* **2022**, *1205*, 339753. [CrossRef] [PubMed]
10. Ter Schiphorst, J.; Saez Castaño, J.; Diamond, D.; Benito López, F.; Schenning, A.P. Light-responsive Materials for Microfluidic Applications. *Lab Chip* **2018**, *18*, 699–709. [CrossRef] [PubMed]
11. Seo, J.; Wang, C.; Chang, S.; Park, J.; Kim, W. A hydrogel-driven microfluidic suction pump with a high flow rate. *Lab Chip* **2019**, *19*, 1790–1796. [CrossRef]
12. Akyazi, T.; Tudor, A.; Diamond, D.; Basabe-Desmonts, L.; Florea, L.; Benito-Lopez, F. Driving flows in microfluidic paper-based analytical devices with a cholinium based poly(ionic liquid) hydrogel. *Sens. Actuators B Chem.* **2018**, *261*, 372–378. [CrossRef]
13. Ren, K.; Zhou, J.; Wu, H. Materials for Microfluidic Chip Fabrication. *Acc. Chem. Res.* **2013**, *46*, 2396–2406. [CrossRef]
14. Tijero, M.; Díez-Ahedo, R.; Benito-Lopez, F.; Basabe-Desmonts, L.; Castro-López, V.; Valero, A. Biomolecule storage on non-modified thermoplastic microfluidic chip by ink-jet printing of ionogels. *Biomicrofluidics* **2015**, *9*, 44124. [CrossRef]
15. Rendl, M.; Bönisch, A.; Mader, A.; Schuh, K.; Prucker, O.; Brandstetter, T.; Rühe, J. Simple One-Step Process for Immobilization of Biomolecules on Polymer Substrates Based on Surface-Attached Polymer Networks. *Langmuir* **2011**, *27*, 6116–6123. [CrossRef] [PubMed]
16. Griffin, K.; Pappas, D. 3D printed microfluidics for bioanalysis: A review of recent advancements and applications. *TrAC Trends Anal. Chem.* **2023**, *158*, 116892. [CrossRef]
17. Ho, C.M.B.; Ng, S.H.; Li, K.H.H.; Yoon, Y. 3D printed microfluidics for biological applications. *Lab Chip* **2015**, *15*, 3627–3637. [CrossRef]
18. Bhattacharjee, N.; Urrios, A.; Kang, S.; Folch, A. The upcoming 3D-printing revolution in microfluidics. *Lab Chip* **2016**, *16*, 1720–1742. [CrossRef] [PubMed]

19. Sedky, M.; Serry, M. High efficiency 3D printed electromagnetic micropump with a synchronous active valve. *Sens. Actuators A* **2022**, *341*, 113570. [CrossRef]
20. Gong, H.; Woolley, A.T.; Nordin, G.P. High density 3D printed microfluidic valves, pumps, and multiplexers. *Lab Chip* **2016**, *16*, 2450–2458. [CrossRef]
21. Amin, R.; Knowlton, S.; Hart, A.; Yenilmez, B.; Ghaderinezhad, F.; Katebifar, S.; Messina, M.; Khademhosseini, A.; Tasoglu, S. 3D-printed microfluidic devices. *Biofabrication* **2016**, *8*, 22001. [CrossRef]
22. Capel, A.J.; Rimington, R.P.; Lewis, M.P.; Christie, S.D. 3D printing for chemical, pharmaceutical and biological applications. *Nat. Rev. Chem.* **2018**, *2*, 422–436. [CrossRef]
23. Garcia-Rey, S.; Gil-Hernandez, E.; Gunatilake, U.B.; Basabe-Desmonts, L.; Benito-Lopez, F. Development of an alginate/TiO_2-based microfluidic biosystem for chrono-sampling and sensing of glucose in artificial sweat. *Sens. Actuators B Chem.* **2023**, *382*, 133514. [CrossRef]
24. Oliveira, J.; Correia, V.; Castro, H.; Martins, P.; Lanceros-Mendez, S. Polymer-based smart materials by printing technologies: Improving application and integration. *Addit. Manuf.* **2018**, *21*, 269–283. [CrossRef]
25. Damiati, L.A.; El-Yaagoubi, M.; Damiati, S.A.; Kodzius, R.; Sefat, F.; Damiati, S. Role of Polymers in Microfluidic Devices. *Polymers* **2022**, *14*, 5132. [CrossRef] [PubMed]
26. Zhang, X.; Li, L.; Luo, C. Gel integration for microfluidic applications. *Lab Chip* **2016**, *16*, 1757–1776. [CrossRef]
27. Suen, J.W.; Elumalai, N.K.; Debnath, S.; Mubarak, N.M.; Lim, C.I.; Reddy, M.M. The Role of Interfaces in Ionic Liquid-Based Hybrid Materials (Ionogels) for Sensing and Energy Applications. *Adv. Mat. Interfaces* **2022**, *9*, 2201405. [CrossRef]
28. Manasa, C.; Basavanna, V.; Ningaiah, S. Ionic Liquid-Based Hybrid Materials: Ionogel Review. *Biointerface Res. Appl. Chem.* **2023**, *13*, 391.
29. Gil-Gonzalez, N.; Akyazi, T.; Castaño, E.; Benito-Lopez, F.; Morant-Miñana, M.C. Eluci-dating the role of the ionic liquid in the actuation behavior of thermo-responsive ionogels. *Sens. Actuator B* **2018**, *260*, 380–387. [CrossRef]
30. Lee, H.Y.; Cai, Y.; Velioglu, S.; Mu, C.; Chang, C.J.; Chen, Y.L.; Song, Y.; Chew, J.W.; Hu, X.M. Thermochromic Ionogel: A New Class of Stimuli Responsive Materials with Super Cyclic Stability for Solar Modulation. *Chem. Mater.* **2017**, *29*, 6947–6955. [CrossRef]
31. Escobedo, P.; Fernández-Ramos, M.D.; López-Ruiz, N.; Moyano-Rodríguez, O.; Martínez-Olmos, A.; de Vargas-Sansalvador, I.M.P.; Carvajal, M.A.; Capitán-Vallvey, L.F.; Palma, A.J. Smart facemask for wireless CO_2 monitoring. *Nat. Commun.* **2022**, *13*, 72. [CrossRef]
32. Cantrell, K.; Erenas, M.; de Orbe-Payá, I.; Capitán-Vallvey, L. Use of the hue parameter of the hue, saturation, value color space as a quantitative analytical parameter for bitonal optical sensors. *Anal. Chem.* **2010**, *82*, 531–542. [CrossRef]
33. Etxebarria-Elezgarai, J.; García-Hernando, M.; Basabe-Desmonts, L.; Benito-Lopez, F. 3D printed high quality benchtop microfluidic devices integrating smart materials as sensors. In Proceedings of the 21th International Conference on Miniaturized Systems for Chemistry and Life Sciences, Micro Total Analysis Systems μ-TAS-2017, Savannah, GA, USA, 22–26 October 2017; pp. 305–306.
34. Czugala, M.; O'Connell, C.; Blin, C.; Fischer, P.; Fraser, K.J.; Benito-Lopez, F.; Diamond, D. Swelling and shrinking behaviour of photoresponsive phosphonium-based ionogel micro-structures. *Sens. Actuator B* **2014**, *194*, 105–113. [CrossRef]
35. Jiang, J.; Xu, X.; Stringer, J. Support Structures for Additive Manufacturing: A Review. *J. Manuf. Mater. Process.* **2018**, *2*, 64. [CrossRef]
36. Hassibi, A.; Manickam, A.; Singh, R.; Bolouki, S.; Sinha, R.; Jirage, K.B.; McDermott, M.W.; Hassibi, B.; Vikalo, H.; Mazarei, G.; et al. Multiplexed identification, quantification and genotyping of infectious agents using a semiconductor biochip. *Nat. Biotechnol.* **2018**, *36*, 738–745. [CrossRef]
37. Mizuta, T.; Sueyoshi, K.; Endo, T.; Hisamoto, H. Ionic liquid-based dye: A "Dyed plasticizer" for rapid and highly sensitive anion optodes based on a plasticized PVC membrane. *Sens. Actuator B* **2018**, *258*, 1125–1130. [CrossRef]
38. Gourishetty, R.; Crabtree, A.M.; Sanderson, W.M.; Johnson, R.D. Anion-selective electrodes based on ionic liquid membranes: Effect of ionic liquid anion on observed response. *Anal. Bioanal. Chem.* **2011**, *400*, 3025–3033. [CrossRef] [PubMed]
39. Gao, L.; Lin, X.; Zheng, A.; Shuang, E.; Wang, J.; Chen, X. Real-time monitoring of intracellular pH in live cells with fluorescent ionic liquid. *Anal. Chim. Acta* **2020**, *1111*, 132–138. [CrossRef]
40. Sabnis, R.W. *Handbook of Acid-Base Indicators*; CRC Press: Boca Raton, FL, USA, 2007. [CrossRef]
41. Liu, Y.; Yue, S.; Wang, Y.-N.; Wang, Y.; Xu, Z.-R. A multicolor-SERS dual-mode pH sensor based on smart nano-in-micro particles. *Sens. Actuators B Chem.* **2020**, *310*, 127889. [CrossRef]
42. Moradi, V.; Akbari, M.; Wild, P. A fluorescence-based pH sensor with microfluidic mixing and fiber optic detection for wide range pH measurements. *Sens. Actuators A Phys.* **2019**, *297*, 111507. [CrossRef]
43. Lu, Y.; Feng, Q.; Zhang, R.; Lu, H.; Su, J.; Cui, Y.; Zhu, L. An online pH detection system based on a microfluidic chip. *Anal. Chim. Acta* **2020**, *1106*, 71–78. [CrossRef]
44. Kulkarni, M.B.; Ayachit, N.H.; Aminabhavi, T.M. Biosensors and Microfluidic Biosensors: From Fabrication to Application. *Biosensors* **2022**, *12*, 543. [CrossRef] [PubMed]
45. Luka, G.; Ahmadi, A.; Najjaran, H.; Alocilja, E.; DeRosa, M.; Wolthers, K.; Malki, A.; Aziz, H.; Althani, A.; Hoorfar, M. Microfluidics Integrated Biosensors: A Leading Technology to-wards Lab-on-a-Chip and Sensing Applications. *Sensors* **2015**, *15*, 30011–30031. [CrossRef] [PubMed]

46. Melnikov, P.V.; Alexandrovskaya, A.Y.; Naumova, A.O.; Arlyapov, V.A.; Kamanina, O.A.; Popova, N.M.; Zaitsev, N.K.; Yashtulov, N.A. Optical Oxygen Sensing and Clark Electrode: Face-to-Face in a Biosensor Case Study. *Sensors* **2022**, *22*, 7626. [CrossRef]
47. Tudor, A.; Saez, J.; Florea, L.; Benito-Lopez, F.; Diamond, D. Poly (ionic liquid) thermo-responsive hydrogel microfluidic actuators. *Sens. Actuator B* **2017**, *247*, 749–755. [CrossRef]